

Parameter dependence of the neutral Higgs boson production and decay in the two Higgs doublet model

Majid Hashemi* and Neda Nobakht†

Physics Department, College of Sciences, Shiraz University, Shiraz, 71946-84795, Iran

In this work, we present a study of the neutral Higgs bosons in the two Higgs doublet model (2HDM) in terms of their production processes and decay channels as a function of the model parameters. The analysis is performed for all four types of the 2HDM and the most promising processes and decay channels are identified for each type of the model. Several Higgs boson mass scenarios below and above the threshold of decay to gauge boson pair are introduced and the corresponding categories of final states are analyzed. It is shown that future lepton colliders have the potential to explore regions in the 2HDM parameter space which are out of the reach of LHC. Final results are presented in terms of the signal cross sections in different final states at relevant center of mass energies of $\sqrt{s} = 365$ GeV at the Future Circular Collider in e^+e^- collision mode (FCC-ee) and $\sqrt{s} = 500$ GeV at the Compact Linear Collider (CLIC) or International Linear Collider (ILC).

INTRODUCTION

One of the main achievements in high energy physics in the last decade is the observation of a new boson at the Large Hadron Collider (LHC) by the two collaborations ATLAS and CMS [1, 2].

The observed particle is the candidate for the missing key element of the standard model, i.e., the Higgs boson, h_{SM} [3–8] and its properties are in reasonable agreement with SM predictions as verified by various analyses at the LHC [9–16].

Within the uncertainty of these measurements, there is still possibility to consider beyond Standard Model (BSM) such as the two Higgs doublet model (2HDM) [17–19] which introduces SM-like Higgs boson candidate together with extra neutral and charged Higgs bosons.

Although 2HDM provides the Higgs sector for supersymmetry in the minimal form (MSSM) [20–22], it is still attractive as a standalone model due to the possibility of better agreement with experimental data [23].

The structure of 2HDM and its parameters provide the possibility to coincide the lightest Higgs boson properties to those of the SM Higgs boson [24]. The heavy neutral CP-even (CP-odd) Higgs bosons $H(A)$ and the two charged Higgs bosons H^\pm are considered as extra Higgs bosons to be observed or excluded in the current or future experiments.

After the discovery of the light Higgs boson candidate, one of the main goals of the ATLAS and CMS collaborations has been the search for the extra Higgs bosons.

The ATLAS collaboration has reported an analysis of $pp \rightarrow A \rightarrow Zh$ [25] where the CP-odd Higgs boson, A , decays to Z boson and 125 GeV Higgs boson. They cover four types of 2HDM based on the Higgs-fermion couplings and results are presented in terms of exclusion contours in the parameter space. These results are confirmed by the

CMS collaboration [26]. The heavy Higgs conversion, i.e., $A \rightarrow ZH$ has been analyzed by the two collaborations CMS [27] and ATLAS [28, 29]. We will discuss about these results in the next sections.

While collision data is taken by the two LHC collaborations CMS and ATLAS, there are ongoing analyses focusing on the possibility of observing extra Higgs bosons at the LHC luminosity upgrade [30, 31] and also future lepton colliders such as CLIC [32, 33], ILC [34], FCC [35] and CEPC [36].

In a number of recent works, we analyzed charged [37–39] and neutral [40–42] Higgs boson production and decay at lepton colliders and provided prospects for their observation in different scenarios using benchmark points in the parameter space. The above analyses were based on the alignment limit [43–45] which is defined as the scenario in which the properties of one of the neutral CP-even Higgs mass eigenstates coincide with those of the SM Higgs boson.

The alignment limit is naturally achieved in the so-called decoupling limit where the masses of other scalar states are large and decouple from the SM-like Higgs boson [46]. However, it is possible to achieve the alignment limit even without decoupling [43–45] which has been the case in our previous studies.

In the current work, we consider the possibility of migrating from the alignment limit and we perform a general scan of the parameter space to analyze the neutral Higgs boson branching ratio of decays. The analysis is not limited to a specific type of the 2HDM and all types are analyzed and compared to reach a conclusion on the choice of the most relevant production process and decay channel for the neutral Higgs bosons in each part of the parameter space.

In what follows, a brief theoretical description of the 2HDM and the software setup used for the analysis are presented. Next, we discuss about the signal processes adopted by LHC collaborations and then present our detailed study of the neutral Higgs boson decay channels in different mass scenarios, theoretical constraints and their

* majid.hashemi@cern.ch

† neda.nobakht@yahoo.com

relevance in each type of the model. The final conclusion for each type of the 2HDM is presented at the end.

I. THE TWO HIGGS DOUBLET MODEL

The SM Higgs Lagrangian is written in the form

$$\mathcal{L} = (\partial_\mu \phi)^\dagger (\partial^\mu \phi) - \mathcal{V}(\phi) \quad (1)$$

where \mathcal{V} is the Higgs potential based on only one Higgs doublet Φ :

$$\mathcal{V} = \mu^2 \Phi^\dagger \Phi + \lambda (\Phi^\dagger \Phi)^2 \quad (2)$$

With this form of the potential, the condition to have non-zero vacuum expectation value for the Higgs field is $\mu^2 < 0$.

The two Higgs doublet model is made as an extension of the SM Higgs sector by introducing two Higgs doublets Φ_1 and Φ_2 .

Writing all possible Lagrangian terms requires additional degrees of freedom. The SM Higgs potential μ^2 term is extended to include three parameters m_{11}^2 , m_{22}^2 and m_{12}^2 and the λ term is extended to seven terms containing λ_1 to λ_7 [46–48]. In such a general Higgs potential, Higgs-boson-associated FCNC interactions exist. It has been shown that such FCNC terms are avoided at tree level by imposing discrete Z_2 symmetry ($\Phi_1 \rightarrow \Phi_1$ and $\Phi_2 \rightarrow -\Phi_2$) [18]. The 2HDM Higgs potential under softly broken Z_2 symmetry (allowing $m_{12} \neq 0$) reduces to the following form [49]:

$$\begin{aligned} \mathcal{V} = & m_{11}^2 \Phi_1^\dagger \Phi_1 + m_{22}^2 \Phi_2^\dagger \Phi_2 - m_{12}^2 (\Phi_1^\dagger \Phi_2 + \Phi_2^\dagger \Phi_1) \\ & + \frac{1}{2} \lambda_1 (\Phi_1^\dagger \Phi_1)^2 + \frac{1}{2} \lambda_2 (\Phi_2^\dagger \Phi_2)^2 \\ & + \lambda_3 (\Phi_1^\dagger \Phi_1) (\Phi_2^\dagger \Phi_2) + \lambda_4 (\Phi_1^\dagger \Phi_2) (\Phi_2^\dagger \Phi_1) \\ & + \frac{1}{2} \lambda_5 \left[(\Phi_1^\dagger \Phi_2)^2 + (\Phi_2^\dagger \Phi_1)^2 \right] \end{aligned}$$

The condition corresponding to the SM $\mu^2 < 0$ is that the Higgs mass matrix made of m_{ij}^2 has at least one negative eigenvalue. If this is the case, the two doublets can be written in terms of their vacuum expectation values:

$$\langle \Phi_1 \rangle = \frac{1}{\sqrt{2}} \begin{pmatrix} 0 \\ v_1 \end{pmatrix}, \quad \langle \Phi_2 \rangle = \frac{1}{\sqrt{2}} \begin{pmatrix} 0 \\ v_2 \end{pmatrix} \quad (3)$$

where the ratio of the two vevs is a free parameter of the model denoted by $\tan \beta = v_2/v_1$ with $v^2 = v_1^2 + v_2^2 = (246 \text{ GeV})^2$.

The other parameter is the mixing angle α used to diagonalize the CP-even Higgs mass-squared matrix. The two parameters α and β appear in the Higgs-fermion and Higgs-gauge couplings [49]. The Higgs-fermion Yukawa

interactions, keeping only the neutral Higgs interactions, take the following form

$$\mathcal{L}_Y = \sum_{f=u,d,\ell} \frac{m_f}{v} \left(\xi_h^f \bar{f} f h + \xi_H^f \bar{f} f H - i \xi_A^f \bar{f} \gamma_5 f A \right) \quad (4)$$

where the couplings are expressed in terms of the corresponding SM value, m_f/v , times the type dependent factors $\xi_{h/H/A}^{u,d,\ell}$ presented in Tab. I. The CP-even Higgs coupling terms are sometimes written in terms of $\sin(\beta - \alpha)$ or $\cos(\beta - \alpha)$ using trigonometric relations [46]:

$$\begin{aligned} \sin \alpha / \sin \beta &= \cos(\beta - \alpha) - \cot \beta \sin(\beta - \alpha) \\ \cos \alpha / \cos \beta &= \cos(\beta - \alpha) + \tan \beta \sin(\beta - \alpha) \\ -\sin \alpha / \cos \beta &= \sin(\beta - \alpha) - \tan \beta \cos(\beta - \alpha) \\ \cos \alpha / \sin \beta &= \sin(\beta - \alpha) + \cot \beta \cos(\beta - \alpha) \end{aligned} \quad (5)$$

The Higgs boson couplings to gauge bosons are model independent and, normalized to their corresponding SM values, are

$$g_{hVV} = \sin(\beta - \alpha), \quad g_{HVV} = \cos(\beta - \alpha). \quad (6)$$

There is no tree level coupling of CP-odd Higgs boson A to vector bosons.

Since $\xi_h^{u,d,\ell}$ is either $\cos \alpha / \sin \beta$ or $-\sin \alpha / \cos \beta$, it is obvious through Eq. 5 and 6 that both h -fermion and h -gauge couplings align to their corresponding SM values if $\sin(\beta - \alpha) = 1$. One of the consequences of the alignment is that the heavier CP-even Higgs coupling to gauge bosons vanishes and its couplings to fermions is expressed in terms of $\tan \beta$ or $\cot \beta$.

The above simplified scheme of Higgs-fermion/gauge couplings has been analyzed in various analyses. The extra Higgs bosons (H and A) are gaugeophobic and their couplings to fermions, normalized to the corresponding SM couplings, depend on β while α is fixed through $\sin(\beta - \alpha) = 1$.

In this work, we do not restrict ourselves to the above requirement and instead, we take $\sin(\beta - \alpha)$ and $\tan \beta$ as input to evaluate the couplings of Tab. I with the use of 2HDMC 1.8 [50–52]. Results are checked to be consistent with the experimental limits using HiggsBounds 5.9.0 [53–57] and HiggsSignal 2.6.0 [58–60] which are embedded in 2HDMC 1.8.0. In addition to the experimental constraints, the theoretical requirements of potential stability (positivity) [61–65], unitarity and perturbativity [66–68] are also verified.

II. THE LHC SEARCH CHANNEL FOR 2HDM NEUTRAL HIGGS BOSONS

Before proceeding to our detailed analysis, we discuss about the LHC (ATLAS and CMS) search channel for the 2HDM neutral Higgs bosons presented in [25–29].

	Type I	Type II	Type III	Type IV
ξ_h^u	$\cos \alpha / \sin \beta$	$\cos \alpha / \sin \beta$	$\cos \alpha / \sin \beta$	$\cos \alpha / \sin \beta$
ξ_h^d	$\cos \alpha / \sin \beta$	$-\sin \alpha / \cos \beta$	$-\sin \alpha / \cos \beta$	$\cos \alpha / \sin \beta$
ξ_h^ℓ	$\cos \alpha / \sin \beta$	$-\sin \alpha / \cos \beta$	$\cos \alpha / \sin \beta$	$-\sin \alpha / \cos \beta$
ξ_H^u	$\sin \alpha / \sin \beta$	$\sin \alpha / \sin \beta$	$\sin \alpha / \sin \beta$	$\sin \alpha / \sin \beta$
ξ_H^d	$\sin \alpha / \sin \beta$	$\cos \alpha / \cos \beta$	$\cos \alpha / \cos \beta$	$\sin \alpha / \sin \beta$
ξ_H^ℓ	$\sin \alpha / \sin \beta$	$\cos \alpha / \cos \beta$	$\sin \alpha / \sin \beta$	$\cos \alpha / \cos \beta$
ξ_A^u	$\cot \beta$	$\cot \beta$	$\cot \beta$	$\cot \beta$
ξ_A^d	$-\cot \beta$	$\tan \beta$	$\tan \beta$	$-\cot \beta$
ξ_A^ℓ	$-\cot \beta$	$\tan \beta$	$-\cot \beta$	$\tan \beta$

TABLE I. Yukawa couplings of the up-type (u) and down-type (d) quarks and leptons (ℓ) to the neutral Higgs bosons $h/H/A$ in different types of 2HDM. There are also other names for types III and IV: flipped and lepton-specific [24].

The above analyses are based on the single CP-odd Higgs boson production followed by the subsequent decay $A \rightarrow ZH$ or $A \rightarrow Zh_{SM}$. The CMS collaboration also considers the $m_H > m_A$ possibility through $H \rightarrow ZA$ decay [27]. In our study, we assume $m_A > m_H$ while analysis of the opposite case can be performed in a similar way.

The LHC searches for the neutral Higgs bosons are divided into two categories of Higgs boson conversion, i.e., $A \rightarrow Zh_{SM}$ and $A \rightarrow ZH$ where the final state contains SM-like Higgs boson or the CP-even heavy Higgs boson.

The decay chains for the two processes are slightly different. The case of $A \rightarrow Zh$ involves $\cos(\beta - \alpha)$ as the coupling factor and vanishes at the alignment limit which is defined as $\cos(\beta - \alpha) = 0$. While the $A \rightarrow Zh$ coupling is type independent, $h_{SM} \rightarrow b\bar{b}$ depends on the type of the 2HDM which results in different patterns for the four types of the 2HDM in two dimensional $\tan \beta$ vs $\cos(\beta - \alpha)$ space.

Figure 1 shows $BR(A \rightarrow Zh) \times BR(h \rightarrow b\bar{b})$ for the four types as a function of $\tan \beta$ and $\cos(\beta - \alpha)$. Except for the lepton-specific type which is essentially designed for $h \rightarrow \ell\bar{\ell}$, any suppression of the product of branching ratios in $A \rightarrow Zh \rightarrow Zb\bar{b}$ which occurs at $\cos(\beta - \alpha) \neq 0$ is due to the suppression of $h \rightarrow b\bar{b}$, otherwise a symmetric pattern around the vertical line of $\cos(\beta - \alpha) = 0$ would have been obtained.

The case of heavy Higgs boson conversion through $A \rightarrow ZH$ analyzed in [27–29] is suitable at the alignment limit as the coupling is $\sin(\beta - \alpha)$. Therefore, for a given $\tan \beta$, the two production processes, i.e., $A \rightarrow ZH$ and $A \rightarrow Zh$ are complementary along the $\cos(\beta - \alpha)$ axis.

Probably one of the reasons for using $A \rightarrow Zh$ by the LHC collaborations has been less number of free parameters in the signal due to the fixed value of h_{SM} mass. Moreover, $A \rightarrow Zh$ can be tested for A masses as low as $m_h + m_Z$ while such masses are not allowed in $A \rightarrow ZH$ due to $m_H > m_h$ assumption. However, as long as the alignment limit and its nearby area is

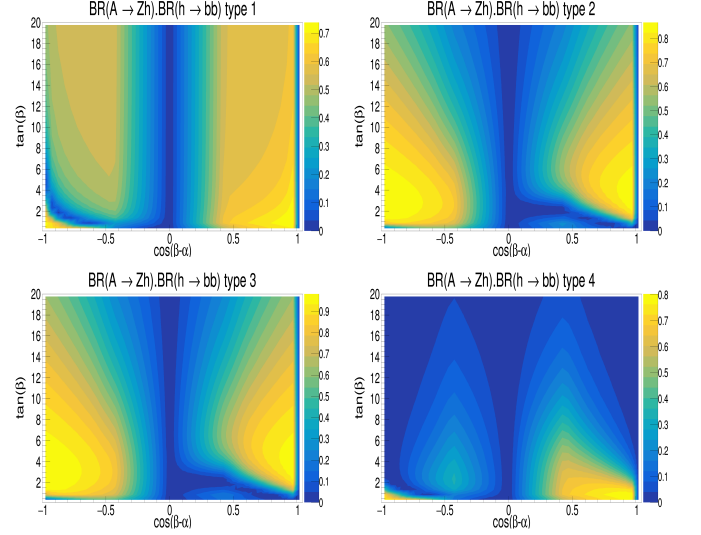


FIG. 1. The product of the branching ratio of the two decay channels adopted by LHC in [25, 26].

concerned, $A \rightarrow ZH$ provides a higher sensitivity near $\cos(\beta - \alpha) = 0$.

There are also differences in the CP-even Higgs boson decays to fermions as well as gauge bosons. Since $h \rightarrow b\bar{b}$ has been analyzed by LHC, we will discuss about $H \rightarrow b\bar{b}$ in the next sections. Concerning the heavy Higgs boson decay to gauge bosons, it was mentioned that the coupling, normalized to the corresponding SM value, is $\cos(\beta - \alpha)$ (Eq. 6). Therefore combining $A \rightarrow ZH$ and $H \rightarrow VV$ ($V = W$ or Z) may not be a reasonable idea as the two coupling factors compensate each other and the higher the production cross section, the lower the $H \rightarrow VV$ decay rate. This is not the case for $A \rightarrow Zh$ followed by $h \rightarrow VV$ as both involve $\cos(\beta - \alpha)$ factors. However, it is essentially a production chain most suitable far from the alignment area. On the other hand, the higher final state particle multiplicity due to gauge boson decays leads to no superiority over fermionic final states.

Therefore the conclusion for both processes ($A \rightarrow ZH$ and $A \rightarrow Zh$) is to preferably use $H/h \rightarrow f\bar{f}$. Here, we denote the decay final state as $f\bar{f}$ to remember that in lepton-specific type, the $\tau\tau$ final state has to be used while in other types $b\bar{b}$ is the most suitable final state of the light or heavy CP-even Higgs boson.

Another possibility, which is currently missing among the list of LHC analyses, is to use single neutral gauge boson production leading to the Higgs boson pair production, i.e., pp or $e^+e^- \rightarrow Z^* \rightarrow AH$. Here we also include lepton collisions at future colliders. The final state can be set by $A \rightarrow b\bar{b}$, $H \rightarrow b\bar{b}$ or $A \rightarrow b\bar{b}$, $H \rightarrow VV$ with b replaced by τ for the lepton-specific type. The $A \rightarrow VV$ can not be considered due to vanishing CP-odd Higgs-gauge coupling. Figures 2 and 3 show the Feynman diagrams related to the Higgs boson pair production in the two final states discussed above. These are example diagrams for lepton pair collision and $V = W$ while

for the case of LHC, the same signal is initiated through quark anti-quark annihilation.

Since the signal is proposed to be analyzed in the four b -jet final state, reasonable control of the QCD background at the LHC event environment is crucial. However, we have shown in a number of analyses that the signal of this process can well be observable at future lepton colliders (the most recent results are found in [69]).

In the following sections, taking the Higgs boson pair production as the golden channel for extra Higgs boson studies, we discuss about the branching ratio of CP-even and CP-odd Higgs boson decays and reach the final conclusion by analyzing all main combinations of decays.

III. CP-EVEN HEAVY HIGGS BOSON DECAY

The Higgs boson pair production should be analyzed in a specific final state. The decay of the CP-even Higgs boson can occur in fermionic mode if the Higgs boson mass is below the threshold of the lightest gauge boson pair production, i.e., if $m_H < 2m_W$. With $m_H > 2m_W$, decay to WW and then ZZ (if $m_H > 2m_Z$) are kinematically allowed. However, one should be aware of possible Higgs boson conversion, i.e., $H \rightarrow hh$, which turns on if $m_H > 2m_h$. Therefore we discuss about the three regions as follows.

A. $m_H < 2m_W$

In this region the Higgs boson decays to fermions, i.e., b quarks in types I to III, and τ leptons in type IV (lepton-specific) unless decay to gauge bosons is enhanced by migrating from the alignment limit.

As seen in Fig. 4, in type I, $H \rightarrow bb$ is dominant near the alignment limit where $H \rightarrow VV$ is suppressed. However, increasing $|\cos(\beta - \alpha)|$ enhances $H \rightarrow VV$ in off-shell mode resulting in reduction of $H \rightarrow bb$ down to 0.2 or lower. However, the lower the Higgs boson mass, the higher the suppression of $H \rightarrow VV$. The two similar types II and III allow $H \rightarrow bb$ to be dominant in a wider area of the parameter space due to the $\tan \beta$ factor in the $H \rightarrow bb$ coupling (Eq. 5). The type IV behaves similar to type I with b replaced by τ . However, contrary to type I in which $H \rightarrow bb$ is almost $\tan \beta$ independent, in type IV, $H \rightarrow \tau\tau$ is enhanced at high $\tan \beta$.

In order to compare the two fermionic and bosonic decay modes, we plot $H \rightarrow WW$ in the same parameter space as shown in Fig. 5. The two complementary plots shown in Figs. 4 and 5 show how the two decay modes $H \rightarrow ff$ and $H \rightarrow WW$ compete. These two plots assume $m_H = 150$ GeV.

Here we verify that the region of parameter space shown in Figs. 4 and 5 is theoretically accessible with no problems of unitarity, stability and perturbativity.

In order to do so, a range of valid m_{12}^2 is found for each point in the parameter space as shown for four chosen

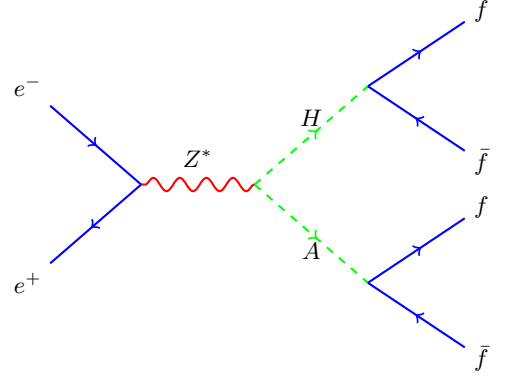


FIG. 2. Higgs boson pair production in the four fermion final state.

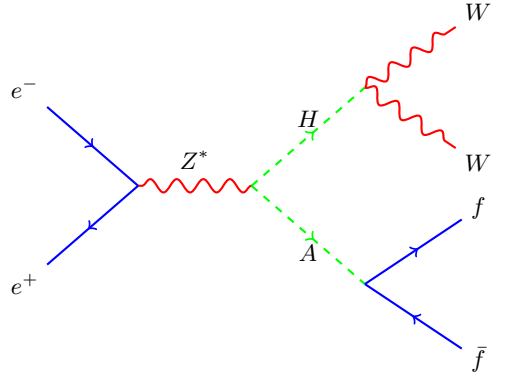


FIG. 3. Higgs boson pair production in $WWff$ channel. Due to the large particle multiplicity in the final state, this channel may not provide better signal significance compared to the four fermion final state.

values of $\tan \beta = 1, 5, 10$ and 20 in Fig. 6. As is seen, increasing $\tan \beta$ shrinks the available m_{12}^2 range for a given point defined by the values of $\cos(\beta - \alpha)$ and $\tan \beta$.

For the mass scenario adopted in this section, $\text{BR}(H \rightarrow ff)$ and $\text{BR}(H \rightarrow VV)$ are independent of m_{12}^2 and any value of m_{12}^2 can be picked up from the range shown in Fig. 6. However, plots shown in Fig. 6 confirm that such m_{12}^2 value always exist for the range of $\tan \beta$ and $\cos(\beta - \alpha)$ under study.

B. $2m_W < m_H < 2m_h$

In this region, $H \rightarrow WW$ starts to occur in on-shell mode and if $m_H > 2m_Z$, $H \rightarrow ZZ$ will also be present. The relevant domain of $H \rightarrow VV$ is limited to Higgs boson masses below the threshold of SM-like Higgs boson pair production, i.e., $2m_W \lesssim m_H \lesssim 2m_h$.

As for illustration, we show $\text{BR}(H \rightarrow ff)$ and $\text{BR}(H \rightarrow WW)$ in Figs. 7 and 8 respectively. The Higgs boson mass is set to $m_H = 200$ GeV. The Higgs boson decay to gauge boson pair is dominant when $|\cos(\beta - \alpha)|$

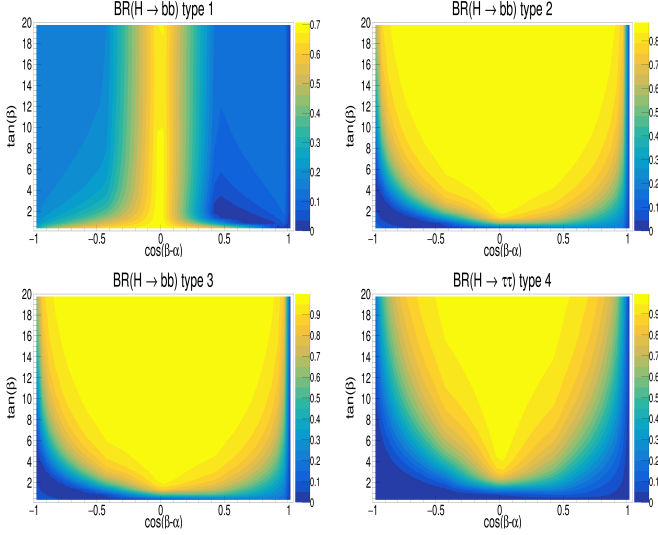


FIG. 4. Branching ratio of Higgs boson decay to fermions (bb final state in types I to III and $\tau\tau$ in type IV). The Higgs boson mass is set to 150 GeV which is near the threshold of on-shell $H \rightarrow WW$. The lower masses lead to $H \rightarrow ff$ dominance in a wider region on both sides of $\cos(\beta - \alpha) = 0$.

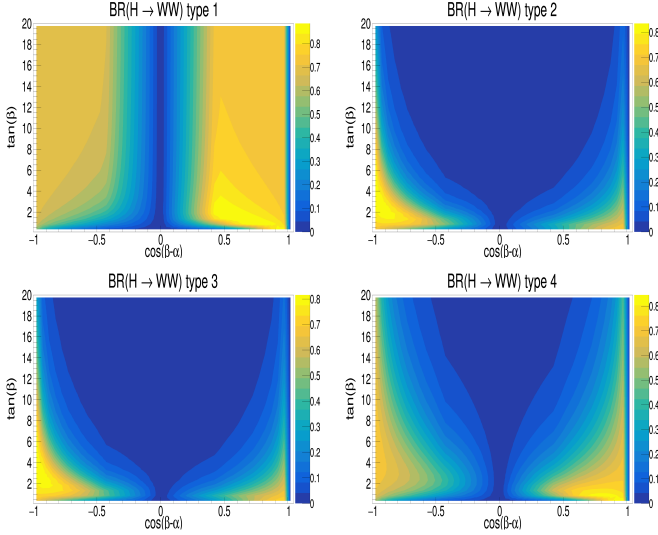


FIG. 5. Branching ratio of Higgs boson decay to W boson pair assuming $m_H = 150$ GeV.

approaches unity unless $H \rightarrow ff$ is enhanced at high $\tan\beta$ values in types II to IV. Inverse colors in the two plots shown in Figs. 7 and 8 show that there is no other relevant decay mode for such Higgs boson masses in the range $2m_W \lesssim m_H \lesssim 2m_h$.

The red hashed region in Figs. 7 and 8 are excluded by theoretical constraints. The approach is the same as what was discussed about in the previous section. For a given $\tan\beta$ value, a range of m_{12}^2 is obtained under theoretical constraints. Fig. 9 shows results for the four

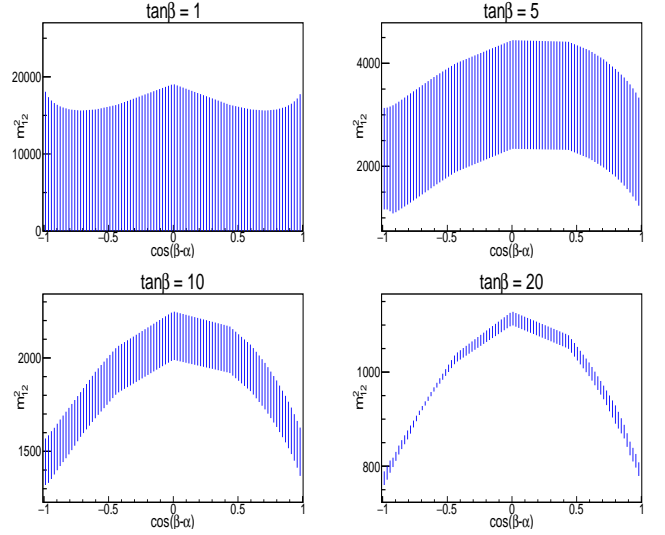


FIG. 6. The valid range of m_{12}^2 as a function of $\cos(\beta - \alpha)$ for four values of $\tan\beta = 1, 5, 10, 20$. The Higgs boson mass is set to $m_{H/A/H^\pm} = 150$ GeV.

values of $\tan\beta$. In this case, at high $\tan\beta$, for some values of negative $\cos(\beta - \alpha)$ there is no m_{12}^2 value respecting theoretical constraints.

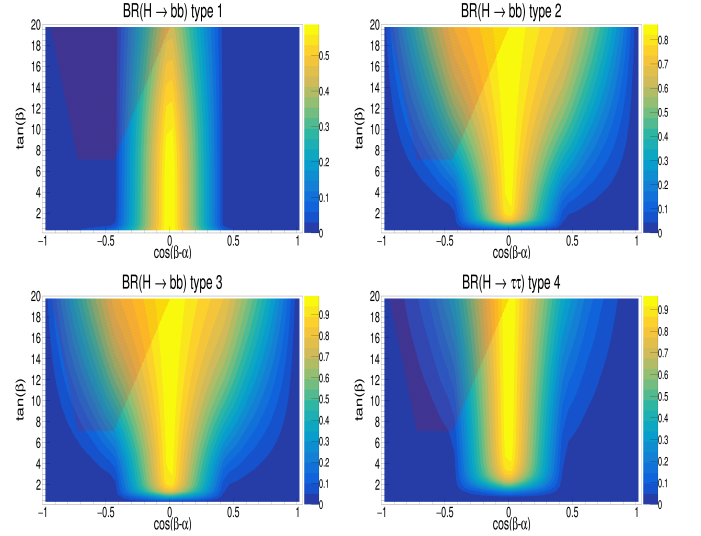


FIG. 7. Branching ratio of Higgs boson decay to fermion pair assuming $m_H = 200$ GeV.

C. $m_H > 2m_h$

If $m_H > 2m_h$, i.e., with a Higgs boson mass above 250 GeV, there is possibility of $H \rightarrow hh$ with a type independent coupling which depends on m_{12}^2 . The presence of this decay mode causes suppression of $\text{BR}(H \rightarrow VV)$. One needs to take care of valid range of m_{12}^2 in terms

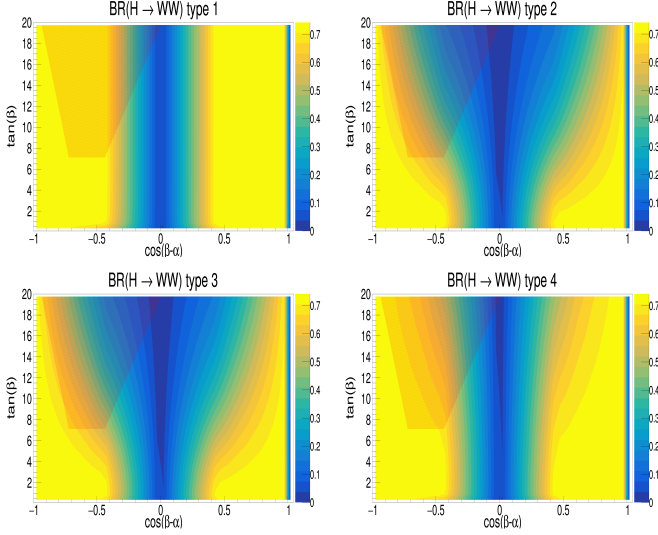


FIG. 8. Branching ratio of Higgs boson decay to W boson pair assuming $m_H = 200$ GeV.

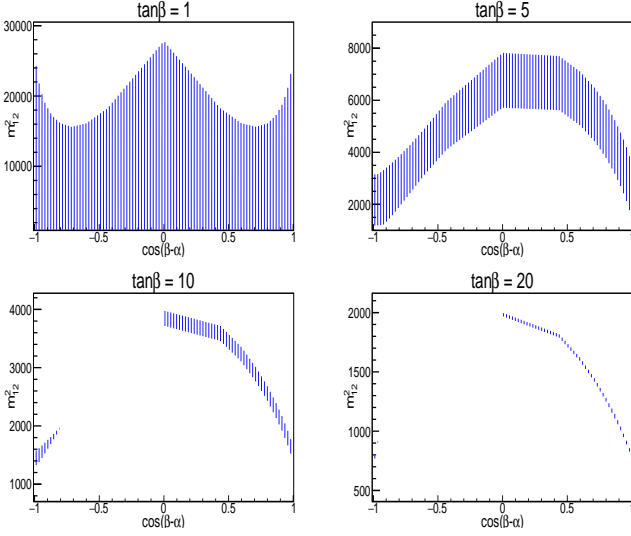


FIG. 9. The valid range of m_{12}^2 as a function of $\cos(\beta - \alpha)$ for four values of $\tan \beta = 1, 5, 10, 20$. The Higgs boson mass is set to $m_{H/A/H^\pm} = 200$ GeV.

of theoretical constraints. On the other hand, m_{12}^2 dependence of the $H \rightarrow hh$ coupling leads to dependence of branching ratio of all other decay modes especially $H \rightarrow VV$ on m_{12}^2 as the sum of all BRs has to be unity.

The only safe area in this mass region is the vertical line of $\cos(\beta - \alpha) = 0$ and nearby where both $H \rightarrow VV$ and $H \rightarrow hh$ are suppressed and there is always a range of m_{12}^2 which respects theoretical constraints. Moreover, due to smallness of the above decay modes in the central region, $\text{BR}(H \rightarrow ff)$ is effectively independent of m_{12}^2 .

Let us show $\text{BR}(H \rightarrow ff)$ in Fig. 10 which features dominance over other decay modes as well as m_{12}^2 independence at the alignment limit.

The m_{12}^2 value has been set to 1000 GeV in Fig. 10. However, m_{12}^2 concerns rise when migrating from the alignment limit where $\text{BR}(H \rightarrow ff)$ is essentially small.

The $\text{BR}(H \rightarrow hh)$ has been shown in Fig. 11 again with fixed value of $m_{12}^2 = 1000$ GeV, which shows that $|\cos(\beta - \alpha)| > 0$ area is under control of this decay mode except for the very low $\tan \beta$ values.

It is notable that there is a larger theoretically excluded area at this mass compared to the lower mass of 200 GeV. The excluded area at negative $\cos(\beta - \alpha)$ is larger and also extends to positive $\cos(\beta - \alpha)$ values at high $\tan \beta$. The dominant decay mode at $|\cos(\beta - \alpha)| > 0.3$ is $H \rightarrow hh$ with $\text{BR}(H \rightarrow hh) > 0.5$. At the central region of $\cos(\beta - \alpha) \simeq 0$, $H \rightarrow bb$ is still dominant as both $H \rightarrow hh$ and $H \rightarrow VV$ are suppressed when approaching this area.

There is a point in Fig. 11 which should be cautious about. We plotted $\text{BR}(H \rightarrow hh)$ for a fixed value of m_{12}^2 to show the relevant domain of this decay mode in the parameter space. However, theoretical constraints rule out some parts of the plot in Fig. 11 because the chosen m_{12}^2 is not in the allowed range. Therefore for each point in the parameter space of $\tan \beta$ vs $\cos(\beta - \alpha)$ a valid m_{12}^2 should be picked up from the specified range to respect the theoretical constraints. The complexity is then due to m_{12}^2 dependence of $\text{BR}(H \rightarrow hh)$ which provides a range of valid branching ratios (not a single value) for each point in Fig. 11.

To conclude, study of $H \rightarrow VV$ at high masses faces difficulties due to theoretical considerations as well as the presence of other decay modes. However, the alignment limit can still be analyzed by $H \rightarrow ff$ at high masses.

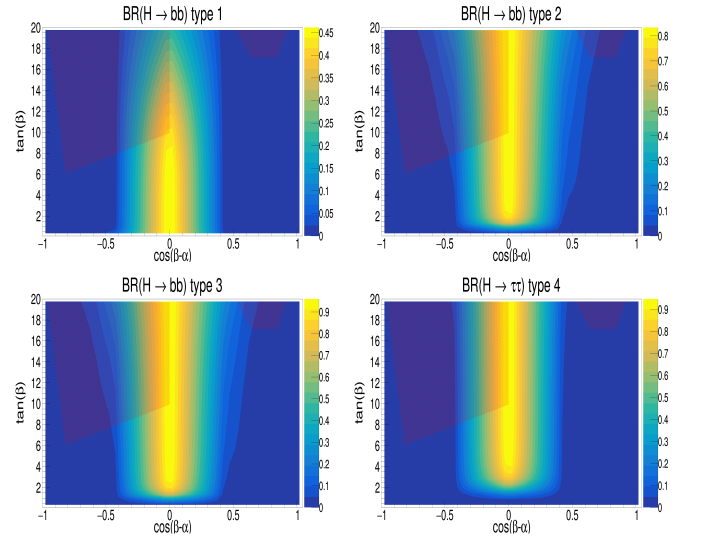


FIG. 10. Branching ratio of Higgs boson decay to fermion pair assuming $m_H = 260$ GeV.

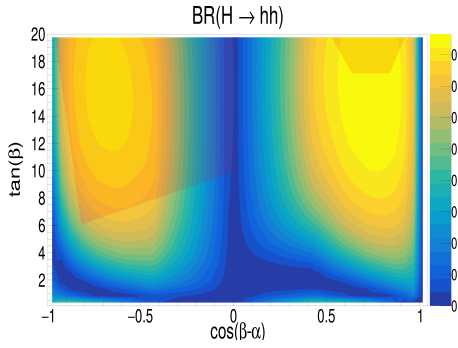


FIG. 11. Branching ratio of Higgs boson decay to SM-like Higgs boson pair assuming $m_H = 260$ GeV.

IV. CP-ODD HEAVY HIGGS BOSON DECAY

The situation with CP-odd Higgs boson decays is simpler as $A \rightarrow VV$ vanishes and $A \rightarrow ff$ depends only on β through $\tan\beta$ or $\cot\beta$. Therefore $\text{BR}(A \rightarrow ff)$ can be plotted as a function of $\tan\beta$ as shown in Figs. 12 and 13 for the two masses $m_A = 150$ and 200 GeV. The main difference between the two masses is observed in type 1, where $A \rightarrow bb$ is more suppressed by $A \rightarrow gg$ at $m_A = 200$ GeV. The other types essentially prefer $A \rightarrow ff$ at $\tan\beta > 5$.

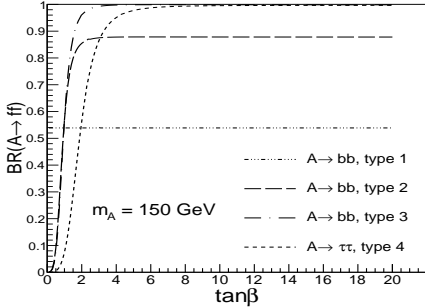


FIG. 12. Branching ratio of CP-odd Higgs boson decay to bb in types 1 to 3 and $\tau\tau$ in type 4. The Higgs boson mass is set to 150 GeV.

V. CROSS SECTION OF THE HIGGS BOSON PAIR PRODUCTION

The only missing element for analyzing the Higgs boson pair production in the final states shown in Figs. 2 and 3 is now the total cross section of HA production which should then be multiplied by branching ratios of Higgs boson decays.

The cross section of these events depends on $\sin(\beta - \alpha)$ through the second vertex and for a fixed value of $\sin(\beta - \alpha)$ is independent of $\tan\beta$. The cross section of the first mass scenario ($m_H = m_A = 150$ GeV) can be calculated

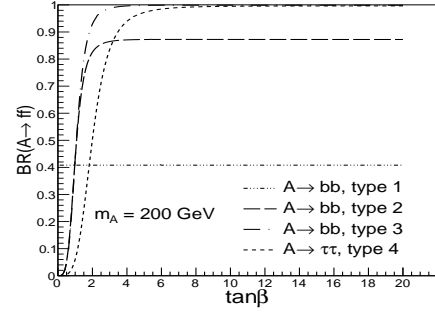


FIG. 13. Branching ratio of CP-odd Higgs boson decay to bb in types 1 to 3 and $\tau\tau$ in type 4. The Higgs boson mass is set to 200 GeV.

for FCC-ee center of mass energy of 365 GeV [70] as well as ILC [71, 72] and CLIC stage 1 [73] operating at center of mass energy of 500 GeV. The second mass scenario above the vector boson pair production threshold can be realized at the same operation scenario of ILC and CLIC.

As previously mentioned, the signal cross section prefers the central region of the alignment due to the $\sin(\beta - \alpha)$ factor thus preferring $H \rightarrow ff$ over $H \rightarrow VV$ because at the alignment limit, in all mass scenarios mentioned before, $H \rightarrow ff$ is dominant.

The final results showing the product of cross sections and branching ratio of CP-even and CP-odd Higgs bosons are presented in Figs. 15 and 16 for FCC-ee center of mass energy $\sqrt{s} = 365$ GeV and Figs. 17 and 18 for CLIC/ILC center of mass energy $\sqrt{s} = 500$ GeV for the two final states $H/A \rightarrow ff$ and $H \rightarrow WW$, $A \rightarrow ff$. The color palette obviously shows that relevant final state for the central region is $H/A \rightarrow ff$ while regions far from the alignment limit can be probed by $H \rightarrow WW$, $A \rightarrow ff$ with its own difficulties.

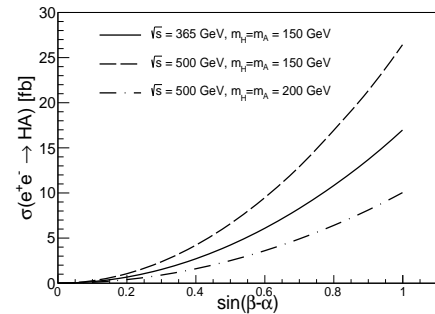


FIG. 14. The signal cross section as a function of $\sin(\beta - \alpha)$ for the two center of mass energies $\sqrt{s} = 365$ GeV (FCC-ee) and 500 GeV (ILC or CLIC). The two scenarios of $m_H = m_A = 150$ GeV and 200 GeV are shown. The signal cross section has a quadratic dependence on $\sin(\beta - \alpha)$ and reaches its maximum at $\sin(\beta - \alpha) = 1$ for each mass scenario.

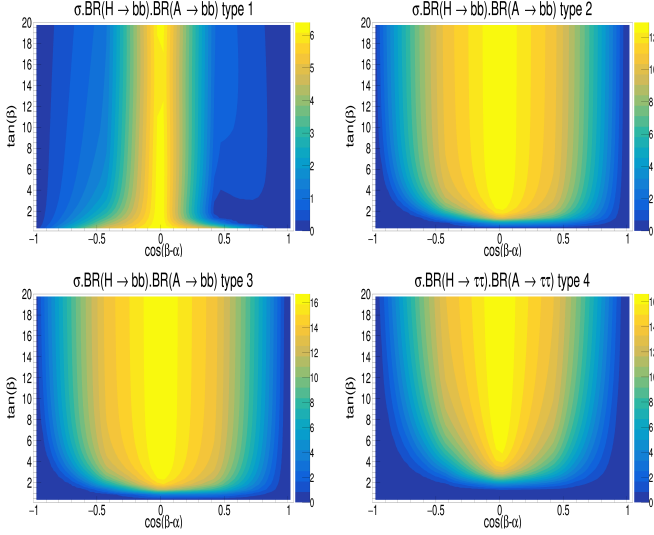


FIG. 15. The signal cross section in the four fermion final state for the mass scenario $m_H = m_A = 150$ GeV at $\sqrt{s} = 365$ GeV.

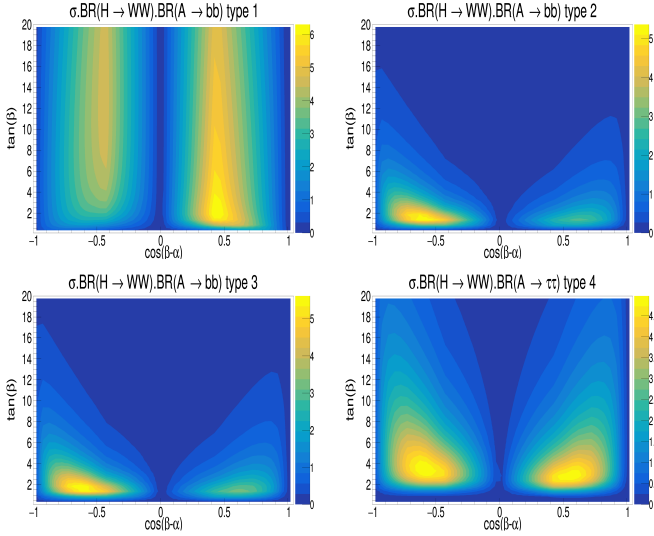


FIG. 16. The signal cross section in the $WWff$ final state for the mass scenario $m_H = m_A = 150$ GeV at $\sqrt{s} = 365$ GeV.

VI. CONCLUSIONS

The two Higgs double model was studied in this work as the theoretical framework for study of extra neutral Higgs bosons in terms of their production processes and decay channels. The analysis was performed for all four types of the CP-conserving 2HDM and parameter space scans were presented including relevant parameters which determine the production cross sections and branching ratio of decays.

The final results were divided into two domains of the Higgs boson mass, i.e., below and above the threshold of decay to gauge boson pair. It was shown that the

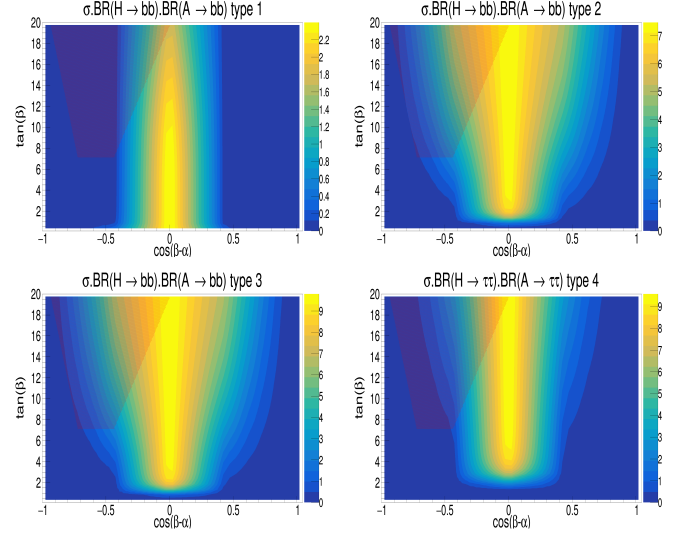


FIG. 17. The signal cross section in the four fermion final state for the mass scenario $m_H = m_A = 200$ GeV at $\sqrt{s} = 500$ GeV.

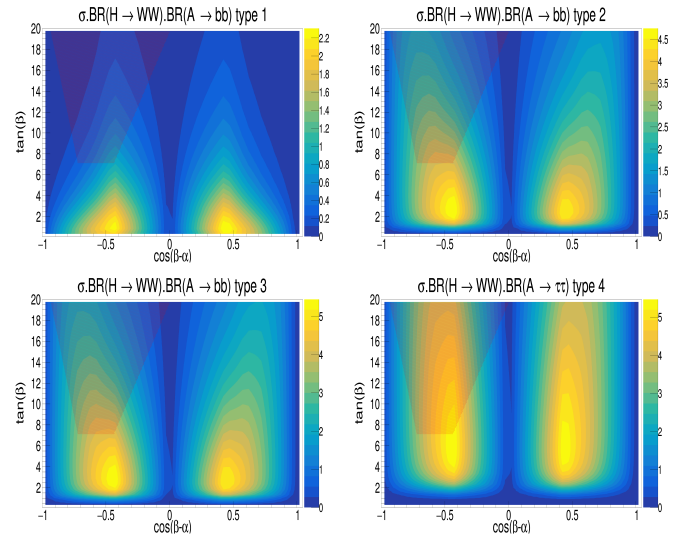


FIG. 18. The signal cross section in the $WWff$ final state for the mass scenario $m_H = m_A = 200$ GeV at $\sqrt{s} = 500$ GeV.

$\cos(\beta - \alpha) = 0$ limit known as the alignment limit can well be verified at lepton colliders if $e^+e^- \rightarrow HA \rightarrow 4$ fermion final state is analyzed. The reason is due to the dominance of the cross section as well as $\text{BR}(H/A \rightarrow ff)$ in this region. The cross sections at FCC-ee center of mass energy of 365 GeV are of the order of 10 fb for the low mass scenario $m_H = m_A = 150$ GeV.

The high mass scenario $m_H = m_A = 200$ GeV is realized at a higher center of mass energy of $\sqrt{s} = 500$ GeV at CLIC or ILC with cross sections of the order of few femtobarns. The other final state, i.e., $e^+e^- \rightarrow HA \rightarrow VVff$, reaches maximum cross section of 6 fb at $\cos(\beta - \alpha) \simeq 0.5$ and low $\tan \beta$ values while one should be aware of the the-

oretical constraints which rule out parts of the parameter space at Higgs boson masses above 200 GeV.

The study presented in this work is not limited to lepton colliders and can be verified at LHC as well. However, the hadronic environment of the LHC events and the large cross section of QCD multi-jet events may reduce the reachable area of the parameter space due to the low signal to background ratio.

At lepton colliders, the 2HDM type 1 has in general lower cross sections compared to other types. We have

shown in [40] that signal cross section of about $4fb$ in 2HDM type 1 (although with slightly different final state from what we propose here) can be observed at $\sqrt{s} = 500$ GeV. We have also analyzed the four b -jet final state in 2HDM type 1 at $\sqrt{s} = 1000$ GeV in [69] and reasonable results have been obtained for the low mass scenarios. Therefore, we expect the parameter space of $\tan\beta$ vs $\cos(\beta - \alpha)$ can be probed at least up to $|\cos(\beta - \alpha)| < 0.5$ thus confirming LHC results and also extending to the untouched alignment limit.

-
- [1] G. Aad et al. (ATLAS), Phys. Lett. **B716**, 1 (2012), 1207.7214.
 - [2] S. Chatrchyan et al. (CMS), Phys. Lett. **B716**, 30 (2012), 1207.7235.
 - [3] P. W. Higgs, Phys. Rev. Lett. **13**, 508 (1964).
 - [4] P. W. Higgs, Phys. Lett. **12**, 132 (1964).
 - [5] P. W. Higgs, Phys. Rev. **145**, 1156 (1966).
 - [6] F. Englert and R. Brout, Phys. Rev. Lett. **13**, 321 (1964).
 - [7] G. S. Guralnik, C. R. Hagen, and T. W. B. Kibble, Phys. Rev. Lett. **13**, 585 (1964).
 - [8] T. W. B. Kibble, Phys. Rev. **155**, 1554 (1967).
 - [9] G. Aad et al. (ATLAS), Phys. Rev. D **101**, 012002 (2020), 1909.02845.
 - [10] G. Aad et al. (ATLAS), Phys. Rev. Lett. **125**, 061802 (2020), 2004.04545.
 - [11] G. Aad et al. (ATLAS), Phys. Lett. B **805**, 135426 (2020), 2002.05315.
 - [12] G. Aad et al. (ATLAS), Eur. Phys. J. C **75**, 476 (2015), [Erratum: Eur.Phys.J.C 76, 152 (2016)], 1506.05669.
 - [13] A. M. Sirunyan et al. (CMS), Phys. Lett. B **792**, 369 (2019), 1812.06504.
 - [14] A. M. Sirunyan et al. (CMS), Eur. Phys. J. C **79**, 421 (2019), 1809.10733.
 - [15] A. M. Sirunyan et al. (CMS), Phys. Rev. Lett. **125**, 061801 (2020), 2003.10866.
 - [16] G. Aad et al. (ATLAS, CMS), JHEP **08**, 045 (2016), 1606.02266.
 - [17] T. D. Lee, Phys. Rev. **D8**, 1226 (1973).
 - [18] S. L. Glashow and S. Weinberg, Phys. Rev. **D15**, 1958 (1977).
 - [19] G. C. Branco, Phys. Rev. **D22**, 2901 (1980).
 - [20] I. J. R. Aitchison (2005), hep-ph/0505105.
 - [21] E. Ma and D. Ng, Phys. Rev. **D49**, 6164 (1994), hep-ph/9305230.
 - [22] A. Djouadi, Phys. Rept. **459**, 1 (2008), hep-ph/0503173.
 - [23] F. Mahmoudi and O. Stal, Phys. Rev. **D81**, 035016 (2010), 0907.1791.
 - [24] G. C. Branco, P. M. Ferreira, L. Lavoura, M. N. Rebelo, M. Sher, and J. P. Silva, Phys. Rept. **516**, 1 (2012), 1106.0034.
 - [25] G. e. a. Aad (ATLAS), Physics Letters B **744**, 163 (2015).
 - [26] A. M. Sirunyan et al. (CMS), Eur. Phys. J. C **79**, 564 (2019), 1903.00941.
 - [27] A. M. Sirunyan et al. (CMS), JHEP **03**, 055 (2020), 1911.03781.
 - [28] M. Aaboud et al. (ATLAS), Phys. Lett. B **783**, 392 (2018), 1804.01126.
 - [29] G. Aad et al. (ATLAS) (2020), 2011.05639.
 - [30] M. Cepeda et al., CERN Yellow Rep. Monogr. **7**, 221 (2019), 1902.00134.
 - [31] H. Bahl, P. Bechtle, S. Heinemeyer, S. Liebler, T. Stefaniak, and G. Weiglein, Eur. Phys. J. C **80**, 916 (2020), 2005.14536.
 - [32] H. Abramowicz et al., Eur. Phys. J. C **77**, 475 (2017), 1608.07538.
 - [33] E. Sicking, Nuclear and Particle Physics Proceedings **273-275**, 801 (2016), ISSN 2405-6014, 37th International Conference on High Energy Physics (ICHEP), URL <https://www.sciencedirect.com/science/article/pii/S2405601415006124>.
 - [34] D. M. Asner et al., in *Community Summer Study 2013: Snowmass on the Mississippi* (2013), 1310.0763.
 - [35] D. d'Enterria, PoS **ICHEP2016**, 434 (2017), 1701.02663.
 - [36] F. An et al., Chin. Phys. C **43**, 043002 (2019), 1810.09037.
 - [37] M. Hashemi, Eur. Phys. J. **C72**, 2207 (2012), 1206.2155.
 - [38] M. Hashemi, Int. J. Mod. Phys. **A27**, 1250165 (2012), 1207.3490.
 - [39] M. Hashemi, Phys. Rev. **D86**, 115002 (2012), 1202.1701.
 - [40] M. Hashemi and G. Haghighat, Eur. Phys. J. C **79**, 419 (2019), 1811.11371.
 - [41] M. Hashemi and G. Haghighat, Phys. Rev. D **100**, 015047 (2019), 1811.12818.
 - [42] M. Hashemi, Phys. Rev. D **98**, 115004 (2018), 1805.10513.
 - [43] J. Bernon, J. F. Gunion, H. E. Haber, Y. Jiang, and S. Kraml, Phys. Rev. D **92**, 075004 (2015), 1507.00933.
 - [44] J. Bernon, J. F. Gunion, H. E. Haber, Y. Jiang, and S. Kraml, Phys. Rev. D **93**, 035027 (2016), 1511.03682.
 - [45] B. Grzadkowski, H. E. Haber, O. M. Ogreid, and P. Osland, JHEP **12**, 056 (2018), 1808.01472.
 - [46] J. F. Gunion and H. E. Haber, Phys. Rev. D **67**, 075019 (2003), hep-ph/0207010.
 - [47] S. Davidson and H. E. Haber, Phys. Rev. **D72**, 035004 (2005), [Erratum: Phys. Rev.D72,099902(2005)], hep-ph/0504050.
 - [48] H. E. Haber and D. O'Neil, Phys. Rev. **D74**, 015018 (2006), [Erratum: Phys. Rev.D74,no.5,059905(2006)], hep-ph/0602242.
 - [49] M. Aoki, S. Kanemura, K. Tsumura, and K. Yagyu, Phys. Rev. **D80**, 015017 (2009), 0902.4665.
 - [50] D. Eriksson, J. Rathsmann, and O. Stal, Comput. Phys. Commun. **181**, 189 (2010), 0902.0851.
 - [51] D. Eriksson, J. Rathsmann, and O. Stal, Comput. Phys. Commun. **181**, 833 (2010).
 - [52] R. Harlander, M. Mühlleitner, J. Rathsmann, M. Spira, and O. Stål (2013), 1312.5571.

- [53] P. Bechtle, O. Brein, S. Heinemeyer, G. Weiglein, and K. E. Williams, *Comput. Phys. Commun.* **181**, 138 (2010), 0811.4169.
- [54] P. Bechtle, O. Brein, S. Heinemeyer, G. Weiglein, and K. E. Williams, *Comput. Phys. Commun.* **182**, 2605 (2011), 1102.1898.
- [55] P. Bechtle, O. Brein, S. Heinemeyer, O. Stål, T. Stefaniak, G. Weiglein, and K. E. Williams, *PoS CHARGED2012*, 024 (2012), 1301.2345.
- [56] P. Bechtle, O. Brein, S. Heinemeyer, O. Stål, T. Stefaniak, G. Weiglein, and K. E. Williams, *Eur. Phys. J. C* **74**, 2693 (2014), 1311.0055.
- [57] P. Bechtle, S. Heinemeyer, O. Stål, T. Stefaniak, and G. Weiglein, *Eur. Phys. J. C* **75**, 421 (2015), 1507.06706.
- [58] P. Bechtle, S. Heinemeyer, O. Stål, T. Stefaniak, and G. Weiglein, *Eur. Phys. J. C* **74**, 2711 (2014), 1305.1933.
- [59] O. Stål and T. Stefaniak, *PoS EPS-HEP2013*, 314 (2013), 1310.4039.
- [60] P. Bechtle, S. Heinemeyer, O. Stål, T. Stefaniak, and G. Weiglein, *JHEP* **11**, 039 (2014), 1403.1582.
- [61] I. F. Ginzburg and I. P. Ivanov (2003), hep-ph/0312374.
- [62] N. G. Deshpande and E. Ma, *Phys. Rev. D* **18**, 2574 (1978).
- [63] B. M. Kastening (1992), hep-ph/9307224.
- [64] J. F. Gunion and H. E. Haber, *Phys. Rev. D* **67**, 075019 (2003), hep-ph/0207010.
- [65] H. E. Haber, in *Joint U.S.-Polish Workshop on Physics from Planck Scale to Electro-Weak Scale (SUSY 94)* (1994), hep-ph/9501320.
- [66] A. Arhrib, in *Workshop on Noncommutative Geometry, Superstrings and Particle Physics* (2000), hep-ph/0012353.
- [67] I. F. Ginzburg and I. P. Ivanov (2003), hep-ph/0312374.
- [68] I. F. Ginzburg and M. Krawczyk, *Phys. Rev. D* **72**, 115013 (2005), hep-ph/0408011.
- [69] M. Hashemi and E. Ebrahimi, *Phys. Rev. D* **103**, 115008 (2021), 2101.00864.
- [70] A. Abada et al. (FCC), *Eur. Phys. J. C* **79**, 474 (2019).
- [71] T. Barklow, J. Brau, K. Fujii, J. Gao, J. List, N. Walker, and K. Yokoya (2015), 1506.07830.
- [72] J. E. Brau, T. Barklow, J. Brau, K. Fujii, J. Gao, J. List, N. Walker, and K. Yokoya (ILC Parameters Joint Working Group), in *Meeting of the APS Division of Particles and Fields* (2015), 1510.05739.
- [73] L. Linssen, A. Miyamoto, M. Stanitzki, and H. Weerts (2012), 1202.5940.